Emergent infinite-randomness fixed points from the extensive random bipartitions of the spin-1 Affleck-Kennedy-Lieb-Tasaki topological state

Min Lu,[1] Wen-Jia Rao,[1] Rajesh Narayanan,[2,3] Xin Wan,[1,4] and Guang-Ming Zhang[5,6]

[1]*Zhejiang Institute of Modern Physics, Zhejiang University, Hangzhou 310027, China*
[2]*Department of Physics, Indian Institute of Technology Madras, Chennai 600036, India*
[3]*Asia Pacific Center for Theoretical Physics, Pohang, Gyeongbuk 790-784, Korea*
[4]*Collaborative Innovation Center of Advanced Microstructures, Nanjing 210093, China*
[5]*State Key Laboratory of Low-Dimensional Quantum Physics and Department of Physics, Tsinghua University, Beijing 100084, China*
[6]*Collaborative Innovation Center of Quantum Matter, Beijing, China*

(Dated: February 11, 2020)

Quantum entanglement under an extensive bipartition can reveal the critical boundary theory of a topological phase in the parameter space. In this study we demonstrate that the infinite-randomness fixed point for spin-1/2 degrees of freedom can emerge from an extensive random bipartition of the spin-1 Affleck-Kennedy-Lieb-Tasaki chain. The nested entanglement entropy of the ground state of the reduced density matrix exhibits a logarithmic scaling with an effective central charge $\tilde{c} = 0.72 \pm 0.02 \approx \ln 2$. We further discuss, in the language of bulk quantum entanglement, how to understand all phase boundaries and the surrounding Griffiths phases for the antiferromagnetic Heisenberg spin-1 chain with quenched disorder and dimerization.

PACS numbers: 75.10.Pq, 03.65.Ud, 03.67.Mn

I. INTRODUCTION

Entanglement spectrum under an extensive bipartition of a topological ground state has recently emerged as a novel approach to study the quantum phase transition between the topological phase and its trivial counterpart.[1–8] The so-called bulk entanglement spectrum (BES) reveals the boundary theory in the corresponding parameter space of a model system, rather than the edge states along the fictitious boundary in real space.[9,10] These studies suggest that a triangular correspondence among the bulk theory, the edge theory, and the critical theory may exist generically for a topological phase.[6,11]

An instructive example is the spin-1 Haldane gapped phase,[12] whose fixed-point properties are captured by the valence-bond solid picture of the Affleck-Kennedy-Lieb-Tasaki (AKLT) model Hamiltonian.[13] The corresponding exact ground state wave function can be expressed as a matrix product state (MPS), indicating that the fundamental entities of the spin-1 chain is actually the fractionalized spinons carrying spin 1/2 that form singlets across adjacent sites. The spin-1/2 object can be observed as the edge mode at the end of the chain, or at the end of a partition in the entanglement study. The degeneracy due to the fractionalized spin in the entanglement spectrum of the antiferromagnetic Heisenberg spin-1 chain is key to understand the Haldane phase as a symmetry protected topological phase.[14] Under a uniform extensive bipartition with disjoint segments, the segment end spins coalesce into an emergent critical spin-1/2 chain with a central charge $c = 1$,[2] which describes the collapse of the Haldane phase under imposed dimerization[8] (marked by the stars in Fig.1).

Meanwhile, spin chains can be interesting with a random probability distribution of the bond couplings between neighboring spins, which may be broaden without limit as the system is coarse-grained.[15] Such a system is governed by the infinite-randomness fixed point (IRFP), whose ground state is characterized by a random pattern of spin singlets formed over large spatial separations.[16,17] For the antiferromagnetic Heisenberg spin-1 chain the Haldane phase is stable against weak disorder[18,19] and weak dimerization,[20] but the emergent critical spin-1/2 chain is not.[16,17] As illustrated in Fig. 1, the Haldane phase and two dimer phases in the presence of quenched disorder are separated by the spin-1/2 random singlet ($RS_{1/2}$) boundaries, which merges into a single spin-1 random singlet (RS_1) boundary between the dimer phases. In addition, unusual Griffiths effects, characterized by two continuously varying dynamical exponents, appear near the boundaries.[21]

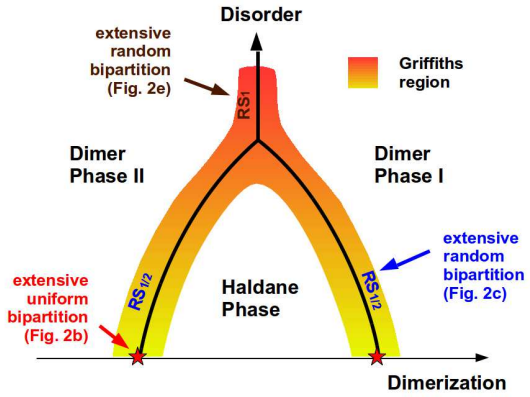

FIG. 1. (Color online) Phase diagram of the antiferromagnetic Heisenberg spin-1 chain in the presence of quenched bond disorder and dimerization.[21] The regimes of interest for the extensive bipartitions in Fig. 2 are labeled accordingly. The red stars mark the critical spin-1/2 chain that can be accessed by the extensive uniform bipartition of the AKLT state.[2] The thick black boundaries are the random singlet states that can be accessed by extensive random bipartitions of the AKLT state (see text).

In this paper we will show that disorder physics can also be revealed in the bulk entanglement study under an extensive random bipartition of the spin-1 chain. For uncorrelated seg-

ment length, the nearest-neighbor couplings in the bulk entanglement Hamiltonian exhibits a power-law distribution, which is precisely the fixed-point solution for random antiferromagnetic spin-1/2 chains under strong-disorder renormalization-group (SDRG) transformation.[17] Therefore, the ground state of the entanglement Hamiltonian realizes the $\mathrm{RS}_{1/2}$ state, for which we provide further evidence by fitting the ensemble-averaged nested entanglement entropy to a logarithmic scaling with an effective central charge $\tilde{c} = 0.72 \pm 0.02 \approx \ln 2$. We discuss how to vary the random bipartition to explore the phase diagram of the antiferromagnetic Heisenberg spin-1 chain with quenched disorder and dimerization.

II. THE AFFLECK-KENNEDY-LIEB-TASAKI SPIN-1 CHAIN

The spin-1 AKLT parent Hamiltonian on a periodic chain of length L is defined by[13]

$$H_{\mathrm{AKLT}} = \sum_{i=1}^{L} J \left[\mathbf{s}_i \cdot \mathbf{s}_{i+1} + \frac{1}{3} \left(\mathbf{s}_i \cdot \mathbf{s}_{i+1} \right)^2 \right], \qquad (1)$$

whose exact ground state can be expressed as an MPS

$$|\Psi_{\mathrm{AKLT}}\rangle = \sum_{\{s_i\}} \mathrm{Tr} \left(\mathbf{A}^{[s_1]} \mathbf{A}^{[s_2]} \cdots \mathbf{A}^{[s_L]} \right) |s_1 s_2 \cdots s_L\rangle ,$$

for $J > 0$, where the local physical spin $s_i = -1, 0, +1$ and $\mathbf{A}^{[s]}$ are local 2×2 matrices given, e.g., in Ref. 2. In the thermodynamic limit, the spin-spin correlation function decays exponentially with a correlation length $\xi = 1/\ln 3 \approx 0.91$, and any two spins that are separated by an even number of the lattice sites are antiferromagnetically correlated.

To study the quantum entanglement of the AKLT state, we can divide the chain into A and B partitions, and define the entanglement Hamiltonian H_E through the reduced density matrix

$$\rho_A = \mathrm{Tr}_B \left(|\Psi_{\mathrm{AKLT}}\rangle\langle\Psi_{\mathrm{AKLT}}| \right) \equiv e^{-H_E}. \qquad (2)$$

In a common practice, as illustrated in Fig. 2a, A is an open spin segment of length $l \geq 2$. The MPS representation dictates that ρ_A contains four eigenvalues: a singlet and a triplet, as required by the SU(2) symmetry. Explicitly, the singlet and triplet eigenvalues are[22,23]

$$\Lambda_0 = \frac{1}{4} \left(1 + 3 \left(-\frac{1}{3} \right)^l \right)$$
$$\Lambda_\alpha = \frac{1}{4} \left(1 - \left(-\frac{1}{3} \right)^l \right), \quad \alpha = 1, 2, 3. \qquad (3)$$

The corresponding entanglement Hamiltonian can thus be determined to be $H_E = J(l) \tau_L \cdot \tau_R$, with

$$J(l) = \ln \left[\frac{1 + 3 \left(-\frac{1}{3} \right)^l}{1 - \left(-\frac{1}{3} \right)^l} \right] \simeq (-1)^l J_0 e^{-l/\xi} \qquad (4)$$

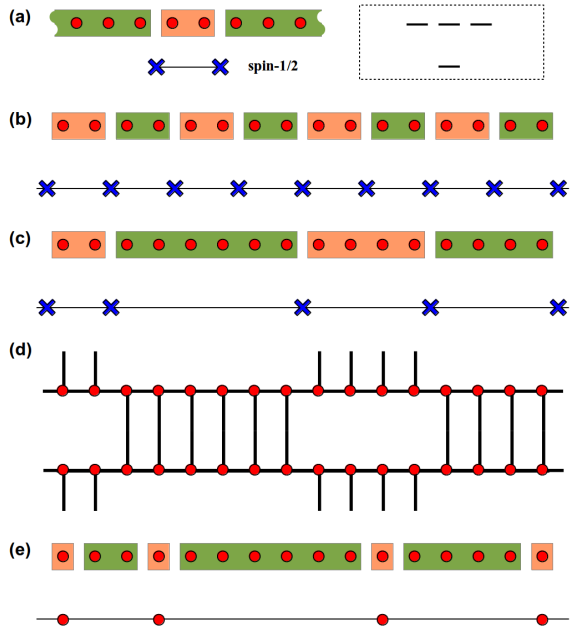

FIG. 2. (Color online) Various bipartitions of the AKLT state and the resulting effective spin models for the entanglement Hamiltonian. We denote A the collection of segments with orange shadow and B that of the segments with green shadow. (a) The entanglement spectrum (illustrated in the box) of a finite segment with an even number of sites is equivalent to the spectrum of two antiferromagnetically coupled spin-1/2s. (b) An extensive uniform bipartition of the AKLT chain (with even-length segments) generates a pure antiferromagnetic spin-1/2 chain, whose ground state can be described by a $c = 1$ CFT. (c) An extensive random bipartition with even-length-only segments generates an effective random antiferromagnetic spin-1/2 chain, whose ground state is the $\mathrm{RS}_{1/2}$ state, and (d) the corresponding ρ_A in the MPS representation. (e) An extensive random bipartition with isolated spins separated by segments of even length generates an effective random antiferromagnetic spin-1 chain, whose ground state is the RS_1 state.

where we have taken the large l limit, and introduced $J_0 = 4$ as the energy unit, $\xi = 1/\ln 3$ is the correlation length, τ_L and τ_R are the two fractionalized spin-1/2s at segment ends. Hence, they are coupled antiferromagnetically for even l, and ferromagnetically for odd l. If we swap A and B, we obtain the identical entanglement Hamiltonian, which means that the coupling between the two end spins is independent of their being connected by a segment in A or by that in B.

On the other hand, the bulk entanglement Hamiltonian H_E stems from the extensive bipartitions that divides the spin chain into A and B sets of alternating segments (see Fig. 2b for an example). The word "bulk" emphasizes that the boundaries between A and B spread out the whole system, and the couplings between the boundary spin-1/2s are relevant. Due to the gap of AKLT model, the coupling strength between spin-1/2s decreases exponentially with their distance, hence only nearest neighboring interactions dominate in large l limit, and the bulk entanglement Hamiltonian is described by the spin-1/2 Heisenberg model, with coupling strength given in Eq. (4).[8] Hence, the H_E with even segment length is critical

and governed by an $SU(2)_1$ Wess-Zumino-Witten conformal field theory (CFT) with central charge $c = 1$. This theory is, however, unstable against arbitrarily small disorder.

III. RANDOM BIPARTITIONING OF THE AKLT CHAIN

A naive thinking to study the effect of quenched disorder is to randomize the bond couplings in the parent Hamiltonian, such that we modify the ground state wave function, hence the reduced density matrix. The AKLT case is, however, an exception. The entanglement spectrum is immune to weak bond randomness [i.e., if we replace uniform J with random J_i in Eq. (1)] as the exact ground state of the random-bond AKLT model is identical to that of the pure model.[13] This is a vivid example that the perturbation can influence thermal excitations but not the excitations in the entanglement spectrum.

This motivates us to enforce disorder by introducing an extensive random bipartition for the AKLT state, as illustrated in Fig. 2c. For the initial simplicity, we assume that the number of lattice sites in each segment is even. After tracing out the degrees of freedom in every other segments, the bulk entanglement Hamiltonian now reduces to a spin-1/2s Heisenberg model with random couplings, that is

$$H_E \simeq \sum_i J_i \tau_i \cdot \tau_{i+1}, \tag{5}$$

where $J_i = J(l_i)$ with l_i being the length of the ith segment, and the form of $J(l)$ is given in Eq. (4). On physical ground we may then expect that the low-energy physics is governed by the IRFP. Normally, this fixed point is revealed by a real-space decimation process, commonly referred to as the SDRG, developed by Dasgupta and Ma[16] and by Fisher.[17] In general, the SDRG process in the initial stage depends strongly on the probability distribution of the random couplings, thus often drives the energy scale of interest to be exponentially small than the strongest bond in the bare Hamiltonian.[24] Surprisingly, this is not the case here because of the uncorrelated locations of the segment ends (which we impose) and the finite correlation length in the topological phase.

For the distribution of segment length (hence the coupling strength), the most natural recipe is to specify a fixed average length of the segments and to assume that the segment ends are located independently. If we suppose that the average length of the segment is large, one can show that the probability distribution of the segment length l (assumed to be continuous for simplicity) satisfies the following differential equation

$$\frac{dP(l)}{dl} = -\frac{P(l)}{\bar{l}}, \tag{6}$$

where the constant $\bar{l}$ is the average length of the segments. We can further assume that the segments have a minimum length of l_0, such that

$$P(l) \sim (1/\bar{l}) e^{-(l-l_0)/\bar{l}}. \tag{7}$$

The discreteness of the segment length is not important when the average segment length is sufficiently long. As often emerged in the minimum mathematical model of the life expectancy problem, the exponential form of the probability distribution simply means that the occurrence of the next segment end is independent of the location of the previous one.

As we discussed above, the energy scale that couples two adjacent segment end spin-1/2s depends on the length of the segment. When the segment length l (measured by the number of sites) is sufficiently long the effective coupling asymptotically approaches Eq. (4). For even l the effective couplings are all antiferromagnetic. We point out, though, including ferromagnetic bonds can lead to a different SDRG fixed point with large spins formed in a random-walk fashion.[25]

The length scales in the two previous exponential laws should in general be different. The former is the average segment length enforced externally, while the latter is the internal correlation length associated with the topological phase. Together, the probability distribution of the effective nearest-neighbor couplings reads

$$P(J) = \frac{1}{\Omega\Gamma}\left(\frac{\Omega}{J}\right)^{1-\frac{1}{\Gamma}}, \tag{8}$$

where $\Gamma = \bar{l}/\xi$ and $\Omega = J_0 e^{-l_0/\xi}$. Once again we stress that, in Eq. (5), the distribution of couplings J_i is random and is given by Eq. (8).

One immediately recognizes that Eq. (8) bears a marked resemblance to the fixed point distribution that describes the random singlet phase in the disordered $S = 1/2$ Heisenberg antiferromagnet, derived by Fisher[16,17] by using a real space based SDRG scheme.

In Fisher's[16,17] SDRG scheme the fixed point distribution that characterizes the random-singlet phase is obtained as the solution of the master equation that describes the flow of the distribution function of coupling constant:

$$\frac{\partial P(\beta)}{\partial \Gamma} = \frac{\partial P(\beta)}{\partial \beta} + P(0)\int_0^\infty d\beta_1 \int_0^\infty d\beta_2 P(\beta_1)P(\beta_2)\delta_{\beta_1+\beta_2-\beta}, \tag{9}$$

where we follow Fisher to introduce the dimensionless scaling variable $\beta = \ln(\Omega/J)$. The differential equation states that during the bond decimation the flow of the bond distribution has two contributions: (i) a shift in β due to the reduction of the UV cutoff Ω, and (ii) the replacement of decimated bonds by the effective couplings generated through the second-order perturbation theory as the logarithmic RG flow parameter Γ changes. As alluded to earlier the Eq. (9) admits a fixed point solution of the form given in Eq. (8). However, at this point it is important to *emphasize* that this striking result elucidated in Eq. (8), is not a result of any SDRG calculation that we have performed but due to the random bipartition scheme that we have adopted wherein the segment lengths are controlled by the distribution given by Eq. (7). We will comment in detail about the apparent similarity of Eq. (7), and the fixed point distribution of the random singlet phase derived by Fisher later on in the manuscript. At this juncture, it suffices to re-emphasize that the extensive bipartition results in

an entanglement Hamiltonian that corresponds to an $S = 1/2$ disordered Heisenberg model.

The ground state entanglement entropy of the random Hesienberg model of Eq. (5) was calculated by Refael and Moore[26] by laying recourse to Fisher's formulation[17] of the SDRG.[16] They realized that the entanglement of a segment of size ℓ with rest of the infinite random Heisenberg chain is just the product of the number of singlet bonds spanning across the boundary times the entanglement entropy per singlet (which is $\ln 2$). To accurately determine the proportionality constant the history of the singlet bond formation across the boundary separating the two subsystems should be kept in detail. In Ref. 26, the SDRG methodology was very successfully adopted to do the same, and it was shown that akin to critical systems, the entanglement entropy in the random-singlet phase of the $S = 1/2$ Heisenberg magnet exhibits a logarithmic scaling with respect to the sub-system size ℓ. In other words,

$$S(\ell) = \frac{\ln 2}{3} \ln \ell + \text{constant}. \tag{10}$$

Here, the coefficient $\ln 2$ that controls the logarithmic behavior is interpreted to be an effective central charge $\tilde{c}$.

Now, in Sec. IV, we will apply the random bipartition scheme and numerically calculate the entanglement entropy of the ground state of the resultant entanglement Hamiltonian. In particular, we compute an effective central charge and compare it to that of the disordered Heisenberg chain $\tilde{c} = \ln 2$ [see Eq. (10) above].

IV. NUMERICAL PROOF

To demonstrate that the IRFP is indeed accessible even in small systems, we study the nested entanglement entropy, a straightforward generalization of the uniform case,[2] and compare it to the entanglement entropy of random $S = 1/2$ Heisenberg chains, which is controlled by an effective central charge $\tilde{c} = \ln 2$.[26] For this purpose, we impose periodic boundary condition and compute ρ_A, whose matrix product representation is illustrated in Fig. 2d, then determine its ground state. We further divided the subsystem A with n segments of a total L_A spin-1s into left partition (p segments) and right partition ($n - p$ segments)

$$\underbrace{l_1, l_2, \cdots, l_p}_{l=\sum_{i=1}^{p} l_i}, \underbrace{l_{p+1}, \cdots, l_n}_{L_A - l} \tag{11}$$

with l and $L_A - l$ spins, respectively. Under this nested bipartition of A, We calculate the nested entanglement entropy $s(l, L_A)$ for the ground state of ρ_A. We average over random realizations of the segment lengths in A and B, among samples with the same number of segments and the same pattern of the nested bipartition, and plot the averaged $\overline{s(l, L_A)}$ as a function of sample averaged $\overline{\ln g(l, L_A)} = \overline{\ln[(L_A/\pi)\sin(\pi l/L_A)]}$ in Fig. 3 for samples with 4-12 segments of random length prescribed by the discrete version of Eq. (7) with $l_0 = 2$ and

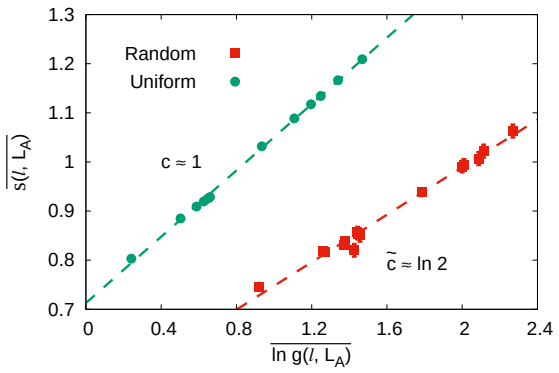

FIG. 3. (Color online) The ensemble-averaged nested entanglement entropy $\overline{s(l, L_A)}$, as a function of the averaged $\overline{\ln g(l, L_A)} = \overline{\ln[(L_A/\pi)\sin(\pi l/L_A)]}$ for the extensive random bipartition, where L_A is the size of A, while l and $L_A - l$ are the sizes of the nested subsystems. The lengths of the segments are chosen according to the discrete version of Eq. (7) with $l_0 = 2$ and $\bar{l} = 5$. We also plot the uniform case[2] for comparison. The slopes of the linear fits are 0.242 ± 0.007 and 0.338 ± 0.004, corresponding to (effective) central charges $\tilde{c} \approx \ln 2$ and $c \approx 1$, respectively.

$\bar{l} = 5 \gg \xi$. Depending on segment number, we choose 2,000-10,000 random realizations. For comparison we also show data for the uniform bipartition with two spins in each segment.[2] The data in the random case can be fitted by

$$\overline{s(l, L_A)} = \frac{\tilde{c}}{3} \overline{\ln \left[\frac{L_A}{\pi} \sin \left(\frac{\pi l}{L_A} \right) \right]}, \tag{12}$$

where the effective central charge $\tilde{c} = 0.72 \pm 0.02$ is in excellent agreement with the expected value of $\ln 2 \approx 0.693$, as oppose to $c = 1$ in the uniform case.[2] The result is remarkable as the largest system contains a mere 12 segments with average segment length $\bar{l} = 5$ and without involving SDRG. The numerical result also demonstrates that the exponentially small longer-range couplings among the segment end spin-1/2s are indeed irrelevant.[17]

The instant arrival at the fixed-point solution of the bulk entanglement Hamiltonian is very reminiscent to the case of the extensive uniform bipartition.[2] For the concrete example in Fig. 2b, one can imagine that a spin-1/2 singlet bond is formed within each segment, leaving an extra pair of spin-1/2s at the two ends to be coupled with the end spins in other segments, as the result of the bipartition. This maps the partition A (a spin-1 chain with bipartition-induced critical dimerization) to a spin-1/2 chain with an effective dimerization $\delta = 0$, since the lengths of A segments and B segments are equal. Therefore, we arrive instantly at the critical point for the pure spin-1 chain with imposed dimerization (i.e., not due to spontaneous symmetry breaking).

Now, in the case of the random bipartition the almost instantaneous arrival at the fixed point solution is also predicated on one another important condition: Namely, our choice of the probability distribution for the segment length [see Eq. (7)]. It is this choice of probability distribution that ensures that our

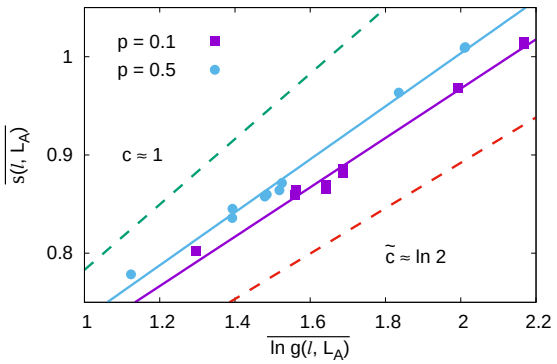

FIG. 4. (Color online) The ensemble-averaged nested entanglement entropy $\overline{s(l,L_A)}$, as a function of the averaged $\overline{\ln g(l,L_A)} = \overline{\ln[(L_A/\pi)\sin(\pi l/L_A)]}$ for binary partition, where L_A is the size of A, while l and $L_A - l$ are the sizes of the nested subsystems. The length of each segment is chosen to be $L_1 = 4$ with probability p or $L_2 = 6$ with probability $1-p$. The effective central charge $\tilde{c}$ can be extracted from the slope to be 0.75 ± 0.03 for $p = 0.1$ and 0.81 ± 0.03 for $p = 0.5$. The values of $\tilde{c}$ are in between $c = 1$ (pure case) and $\tilde{c} = \ln 2$ (IRFP) as indicated by the two dashed lines (guide to eye only).

results immediately converge to the fixed point distribution $P(J)$ for the nearest-neighbor coupling elucidated in Eq. (8). Consequently, the random bipartition effectively sets up the bond distribution that looks akin to the fixed point distribution that characterizes the random singlet phase of the $S = 1/2$ Heisenberg antiferromagnet. This provides a reason of why the numerically computed effective central charge $\tilde{c}$ is almost bereft of finite size effects and locks on immediately to the universal value of $\ln 2$. Of course, this brings out immediately the question of how quickly one can arrive at the random singlet state fixed point if we were to start with a distribution that is non-Poissonian. We defer this discussion to the subsequent paragraph. We end this paragraph with a few comments on the Poissonian distribution of segment length, Eq. (7). In our analysis we have ignored the fact that the segment length is discrete. This can be justified if we imagine approaching the fixed point via an SDRG: Under this SDRG, the ($\sim 1/J$) grows without limit, which means that the system flow to infinite randomness. In our setup this points our primary interest to the regime where $\bar{l}$ is large, hence our assumption that the discreteness of the segment length is not important and our simplification of the length dependence of the effective couplings $J(l)$ between the segment end spins are justified. In the same limit the choice of l_0, which sets the UV cutoff, is also not important.

To understand how the distance to the random singlet state depends on the segment length distribution, we consider a binary partition. The length of each segment is chosen to be L_1 with probability p or L_2 with probability $1-p$ (with $p \leq 0.5$). Apparently, the binary distribution is not desirable as the initial distribution for an SDRG, as the probability that two neighboring lengths are equal can be high. Hence, the perturbative decimation is not valid. While it seems counterintuitive, one can argue that the binary distribution with a smaller p is closer to the IRFP distribution than that with a larger p. The argument goes as follows: With a small p, we expect (with high probability) to have consecutive segments of length L_2 followed by a single segment of length L_1, then another consecutive segments of length L_2 followed by a single segment of length L_1, and so on. In the limit of small p, the number of consecutive length-L_2 segments N has a broad distribution (Poisson, indeed). Within a consecutive length-L_2 segments (say, of total length NL_2), we have effectively $N+1$ antiferromagnetically coupled segment-end spin-1/2s, with low-energy excitations being magnons with energy scale $O(J_0 e^{-L_2/\xi}/N)$. Consequently, a broader distribution of energy scales exists naturally in the entanglement Hamiltonian for smaller p. The argument works well for $L_1 \gg L_2$, when consecutive segments of L_2 are coupled weakly. Nevertheless, even for $L_1 < L_2$, the conclusion is still valid, as the end spin-1/2s of the L_1 segments form singlets and generate much weaker couplings between their neighboring segment-end spins. In Fig. 4, we plot the ensemble-averaged nested entanglement entropy $\overline{s(l,L_A)}$, as a function of the averaged $\overline{\ln g(l,L_A)} = \overline{\ln[(L_A/\pi)\sin(\pi l/L_A)]}$ for the binary partition with $p = 0.1$ and 0.5. We choose $L_1 = 4 < L_2 = 6$ and find that the effective central charge $\tilde{c} = 0.75 \pm 0.03$ for $p = 0.1$ and $\tilde{c} = 0.81 \pm 0.03$ for $p = 0.5$. We list the effective central charge $\tilde{c}$ for five different p in Table I. As expected, the smaller p is, the closer $\tilde{c}$ is toward $\ln 2$ for the IRFP value. On the other hand, the larger p is, the closer $\tilde{c}$ is toward 1 for the disorder-free value. We note that, as we have only up to 12 segments, finite-size artifacts can become significant for $p \leq 0.1$ so $\tilde{c} = \ln 2$ cannot be obtained in our calculation for binary partition.

p	0.1	0.2	0.3	0.4	0.5
$\tilde{c}$	0.75	0.75	0.76	0.77	0.81
Δ_c	0.03	0.04	0.03	0.04	0.03

TABLE I. The effective central charge $\tilde{c}$ with uncertainty Δ_c for binary partition. The length of each segment is chosen to be $L_1 = 4$ with probability p or $L_2 = 6$ with probability $1-p$.

V. DISCUSSIONS AND CONCLUSIONS

The entanglement-revealed criticality in both the pure case and the random case establishes that exploring the appropriate bulk entanglement Hamiltonian of the ground state wave function representing a topological phase can efficiently distill the quantum information belonging to the corresponding critical point separating the topological phase and its adjacent trivial phase. This is also observed for the integer quantum Hall transitions that can be classified by a $\mathbb{Z}$ index.[6]

The distribution of the segment lengths can introduce additional relevant perturbations for the emergent degrees of freedom. One example is that the difference between the average segment lengths in A and B can introduce an effective dimerization δ for the $\mathrm{RS}_{1/2}$ state. Unlike the pure case, δ can be

continuously tuned in the random case. The resulting bulk entanglement Hamiltonian effectively describes random spin-1/2 chains with weak but continuously varying bond dimerization. This can lead to critical behavior but with finite spin correlation length controled by δ, the characteristics of a Griffiths phase.[28] On the other hand, the random antiferromagnetic $S = 1$ chains with enforced dimerization also contain spin-1 degrees of freedom, which, together with the spin-1/2 degrees of freedom, result in Griffiths phases with two independent dynamical exponents. The entanglement analogy, thus, requires that partition A (or B) should contain segments with odd length. We leave the details aside but point out that one can compare the extensive random bipartition case to the domain-wall description of Damle and Huse,[29] hence the relevant physics will follow.

It is interesting to point out that a spin-1 random singlet phase without dimerization[18] can also be accessed, e.g., by a bipartition (see Fig. 2e) that contains single sites in A (creating effective spin-1s) and segments with random but even length in B (providing random antiferromagnetic couplings between effective spin-1s). Indeed, it can be shown the entanglement Hamiltonian is dominated by the antiferromagnetic Heisenberg coupling between nearest neighboring spin-1s. This, however, does not fit the scenario that we discussed above, because the RS_1 state, as illustrated in Fig. 1, is a critical line that is separated from the Haldane phase (including the Griffiths region) by a multicritical point. The multicritical point has an emergent permutation symmetry corresponding to the interchange of the Haldane phase and the dimer phases that meet at the point.[29] We leave it to future investigation whether it is possible to incorporate the permutation symmetry and to access the multicritical point.

In summary, we have discussed how to understand the critical phase boundaries of the antiferromagnetic Heisenberg spin-1 chain in the presence of quenched disorder and dimerization in terms of quantum entanglement by applying extensive bipartitions to the AKLT state that represents the topological Haldane phase. In particular, the calculation of the effective central charge provides a striking example how efficient quantum entanglement can access the critical information of a topological quantum phase transition.

VI. ACKNOWLEDGEMENTS

This work is supported by the 973 Program under Project No. 2012CB927404 and NSF-China through the grants No. 20121302227 and No. 11174246. X.W. acknowledges the hospitality of the Department of Physics at the India Institute of Technology Madras during the course of this work. RN acknowledges funding from the Visitor program at APCTP and also acknowledges support through NRF funded by MSIP of Korea (2015R1C1A1A01052411).

[1] T. H. Hsieh and L. Fu, Phys. Rev. Lett. **113**, 106801 (2014).
[2] W. J. Rao, X. Wan, and G. M. Zhang, Phys. Rev. B **90**, 075151 (2014).
[3] J. Borchmann *et al.*, Phys. Rev. B **90**, 235150 (2014).
[4] T. H. Hsieh, L. Fu, and X. L. Qi, Phys. Rev. B **90**, 085137 (2014).
[5] R. A. Santos, J. Phys. A: Math. Theor. **48**, 155203 (2015).
[6] Q. Zhu, X. Wan, and G. M. Zhang, Phys. Rev. B **90**, 235134 (2014).
[7] S. Vijay and L. Fu, Phys. Rev. B **91**, 220101(R) (2015).
[8] W. J. Rao, G. M. Zhang and K. Yang, Phys. Rev. B **93**, 115125 (2016).
[9] H. Li and F. D. M. Haldane, Phys. Rev. Lett. **101**, 010504 (2008).
[10] X. L. Qi, H. Katsura, and A. W. W. Ludwig, Phys. Rev. Lett. **108**, 196402 (2012).
[11] X. Chen, F. Wang, Y. M. Lu, and D. H. Lee, Nucl. Phys. B **873**, 248 (2013).
[12] F. D. M. Haldane, Phys. Lett. **93A**, 464 (1983); Phys. Rev. Lett. **50**, 1153 (1983).
[13] I. Affleck, T. Kennedy, E. H. Lieb, and H. Tasaki, Phys. Rev. Lett. **59**, 799 (1987); Commun. Math. Phys. **115**, 477 (1988).
[14] F. Pollmann, A. M. Turner, E. Berg, and M. Oshikawa, Phys. Rev. B **81**, 064439 (2010).
[15] See references in D. Huse, Phys. Rep. **348**, 159 (2001).
[16] C. Dasgupta and S. K. Ma, Phys. Rev. B **22**, 1305 (1980).
[17] D. S. Fisher, Phys. Rev. B **50**, 3799 (1994).
[18] R. A. Hyman and K. Yang, Phys. Rev. Lett. **78**, 1783 (1997).
[19] C. Monthus, O. Gollineli, and Th. Jolicoeur, Phys. Rev. Lett. **79**, 3254 (1997); Phys. Rev. B **58**, 805 (1998).
[20] I. Affleck and F. D. M. Haldane, Phys. Rev. B **36**, 5291 (1987).
[21] K. Damle, Phys. Rev. B **66**, 104425 (2002).
[22] H. Fan, V. Korepin, and V. Roychowdhury, Phys. Rev. Lett. **93**, 227203 (2004).
[23] H. Katsura, T. Hirano, and Y. Hatsugai, Phys. Rev. B **76**, 012401 (2007).
[24] X. Wan, K. Yang, and R. N. Bhatt, Phys. Rev. B **66**, 014429 (2002).
[25] E. Westerberg, A. Furusaki, M. Sigrist, and P. A. Lee, Phys. Rev. Lett. **75**, 4302 (1995).
[26] G. Refael and J. E. Moore, Phys. Rev. Lett. **93**, 260602 (2004).
[27] Nicolas Laflorencie, Phys. Rev. B**72**, 140408(R), 2005.
[28] R. A. Hyman, K. Yang, R. N. Bhatt, and S. M. Girvin, Phys. Rev. Lett. **76**, 839 (1996).
[29] K. Damle and D. A. Huse, Phys. Rev. Lett. **89**, 277203 (2002).